1997

Separation and Artificial Maturation of Macerals from Type II Kerogen

Michael A. Kruge
Montclair State University, krugem@mail.montclair.edu

Patrick Landais
CRNS-CREGU

David F. Bensley
Southern Illinois University Carbondale

B Artur Stankiewicz
Southern Illinois University Carbondale

Marcel Elie
CRNS-CREGU

See next page for additional authors

Preprint: Kruge M. A., Landais P., Bensley D. F., Stankiewicz B. A., Elie M., Ruau O. (1997) Separation and artificial maturation of macerals from Type II kerogen. *Energy & Fuels* **11**:503-514.
https://pubs.acs.org/doi/10.1021/ef960191k
https://doi.org/10.1021/ef960191k

Separation and Artificial Maturation of Macerals from Type II Kerogen

M. A. Kruge[1,2], P. Landais[2], D. F. Bensley[1,3], B. A. Stankiewicz[1,4], M. Elie[2], O. Ruau[2]

[1]Dept. of Geology, Southern Illinois Univ., Carbondale, IL 62901 USA. [2]CNRS-CREGU, BP 23, 54501 Vandœuvre-lès-Nancy, France. [3]Carbon Consultants International, Inc., Box 819, Carbondale, IL 62903 USA. [4]Biogeochemistry Research Centre, Dept. of Geology, Univ. of Bristol, Bristol, BS8 1RJ, UK

Abstract: Immature Type II kerogen (HI= 660 mg/g) from the Lower Toarcian of the Paris Basin was separated into an alginite concentrate (HI = 952 mg/g) and an amorphous organic matter (AOM) concentrate (HI = 573 mg/g) by density centrifugation. The flash pyrolyzate of the alginite is characterized by high relative concentrations of several series of *n*-alkanones and *n*-alkenones (including mid-chain alkyl ketones), in addition to *n*-alkanes, *n*-alk-1-enes and *n*-alkadienes. To our knowledge, this Toarcian alginite is the oldest example of marine organic matter whose pyrolyzate contains mid-chain alkanones in such high relative concentrations. In sharp contrast, the AOM produced predominantly alkylbenzenes, alkylthiophenes, *n*-alkanes and *n*-alk-1-enes upon pyrolysis. Micro-FTIR spectroscopy indicated that the alginite was enriched in aliphatic C-H (particularly CH_2) and depleted in aromatic C=C, relative to the AOM, consistent with the pyrolysis results. Aliquots of the concentrates were heated separately in gold tubes (24 h, 70 MPa) at fixed temperatures ranging between 250 and 375°C. Yields of liquid products as a function of temperature were initially greater for the AOM, reaching a maximum at 325°C. In contrast, the alginite yielded little liquid product at low temperatures, attaining its maximum at 350°C, at which temperature its yield greatly surpassed that of the AOM. This kerogen is a heterogeneous assemblage of fossil organic matter, exhibiting different degrees of preservation and petroleum potential. The alginite is fossilized marine algaenans with alkyl chains cross-linked by ether bridges, while the AOM component is at least in part a "geopolymer" with thioether linkages, the thermally labile nature of which is responsible for its lower temperature peak liquid generation. It is evident that the alginite concentrate is chemically distinct from its companion AOM in this kerogen and that the full extent of its uniqueness would not have been revealed without the density separation step.

Introduction

As the heterogeneous, polymeric nature of most sedimentary organic matter greatly complicates its chemical analysis, any successful subdivision into components (macerals) or groups of components may aid in elucidation of chemical structures. While in-situ analytical techniques, such as micro-FTIR[1] and laser micropyrolysis[2], offer some advantages, physical separation by density still provides the best method for preparing milligram to gram quantities of reasonably pure macerals for chemical analysis and experimentation. It would be desirable through the chemical analysis of maceral concentrates to be able to unify the view of kerogen long held by microscopists as a variable assemblage of diverse fossil organic matter (for a review see Teichmüller[3]) with the more recent concept of resistant biopolymers proposed by geochemists[4-6]. Recent advances in extending the resistant biopolymer concept to marine organic matter have come with experiments performed on extant organisms[7-10] and on stratigraphically variable assemblages within the same ancient sedimentary sequences[11,12]. Although they are among the most difficult macerals to separate by density[13-15], alginites from marine kerogens have recently been successfully isolated[14,16].

Presuming the availability of marine kerogen macerals in sufficient quantity, it would be of interest to examine their individual responses to thermal stress, to better understand the oil generating process. Artificial maturation studies have traditionally used whole kerogen, coal or source rock as starting materials for heating experiments[17-19]. Artificial coalification of the macerals isolated from humic coal demonstrated that each maceral responds differently to thermal stress[20-22]. In a companion study to this project, we subjected alginite and organic groundmass isolated from two torbanite samples to artificial maturation experiments[23], with the results that the generation profiles of both maceral types had distinctly different slopes and amplitudes.

As with the companion study on lacustrine organic matter[23], the objectives of this investigation on marine kerogen macerals were two-fold. Our intentions were to document the chemical differences between the alginite and amorphous organic matter, relating them to their different biological precursors, preservation modes and diagenetic pathways. We also sought to test the hypothesis that the diverse organic components of the kerogen should respond differently to the same thermal stimulation.

Experimental Section

Sample. For these experiments, we chose a sample of the classic Type II kerogen from the Lower Toarcian shale of the Paris Basin, France, taken from a drill core at a proprietary location. The shale sample contains 3.54% total organic carbon. Its low, pre-oil window maturity level is confirmed by the presence of sterenes, hopenes and 17β,21β(H) hopanes in its solvent extract. Its kerogen was

petrographically determined to consist of 20% bright yellow-fluorescing lamalginite, 60% dull yellowish orange-fluorescing amorphous organic matter (AOM), 10% vitrinite and 10% inertinite, using reflected white and blue light (Figure 1). It has an atomic H/C ratio of 1.18 and O/C of 0.13, consistent with its designation as immature Type II [24]. The kerogen's Rock Eval hydrogen index of 660 mg pyrolyzate/g C_{org} indicates its high petroleum potential[25]. The sample was chosen because of its relatively high alginite and AOM contents, making it a suitable candidate for procedures to isolate these components, which are the two petrographic constituents most important in petroleum generation from marine kerogens[3].

Maceral separation. Concentrates of the alginite and AOM from both samples were prepared from CH_2Cl_2-extracted, demineralized kerogen by density separation using methods described previously[14,16,23,26,27]. In brief, the sample was crushed to <75 μm size and extracted with excess CH_2Cl_2 in a sonicator, repeating with fresh solvent until clear. Extraction residues were demineralized using 20% HCl followed by 48% HF. The residues after acid treatment were centrifuged in an aqueous CsCl solution with a density of 1.6 g/mL to separate pyrite and remaining silicates from the organic matter. After the sample was washed and dried, it was treated with liquid nitrogen to induce fracturing in the ductile liptinitic macerals, which allows for easier breakage during micronization[14]. The kerogen concentrate thus prepared was reduced nearly to micron size in a Garlock FMT mill at 20°C in a nitrogen atmosphere[14]. The concentrates were extracted again with CH_2Cl_2.

An aliquot (2 g) of the extracted, micronized residue was suspended in water by means of an ultrasonicator and layered on the top of a CsCl density gradient (1.00-1.60 g/mL), following published methodology[28-31]. Petrographic pellets of the fractions were examined and it was determined that high purity lamalginite was found in density fractions in the 1.00-1.11 g/mL range, shown as a low shoulder in Figure 2. The AOM, the most abundant component of this kerogen, produced a strong peak on the DGC profile in the 1.18-1.23 g/mL range. Using the above density ranges as cut points, the remaining kerogen concentrate was centrifuged sequentially in several CsCl solutions of single densities to isolate the alginite and AOM, yielding several hundred mg of each fraction. These two end products were again extracted with CH_2Cl_2 and examined petrographically for purity confirmation. Although the OM particles were reduced to the 10 μm size range during processing, diagnostic petrographic features (fluorescence color and intensity under blue light and reflectivity under white light) were still recognizable. The alginite concentrate was thus determined to be *ca*. 95 vol. % alginite with about 5% of AOM contamination, while the AOM concentrate was found to be about 95 vol. % AOM with 5% vitrinite.

Figure 1. Photomicrograph of the Lower Toarcian kerogen concentrate (reflected blue light) showing bright yellow fluorescing (λ_{max}: 550-560 nm) lamalginite (ALG) and dull orange-yellow fluorescing (λ_{max}: 580-590 nm) degraded, amorphous organic matter (AOM). Non-fluorescing mounting medium appears black. The lamalginite appears contorted due to mechanical deformation during sample processing.

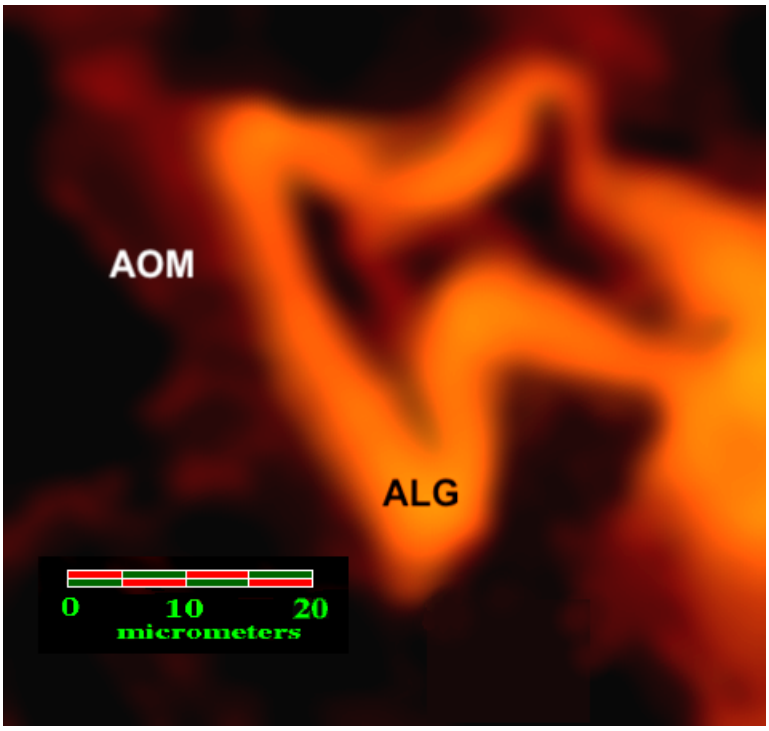

Figure 2. Density gradient centrifugation results for the Lower Toarcian kerogen sample, showing density ranges used in preparation of alginite and AOM concentrates.

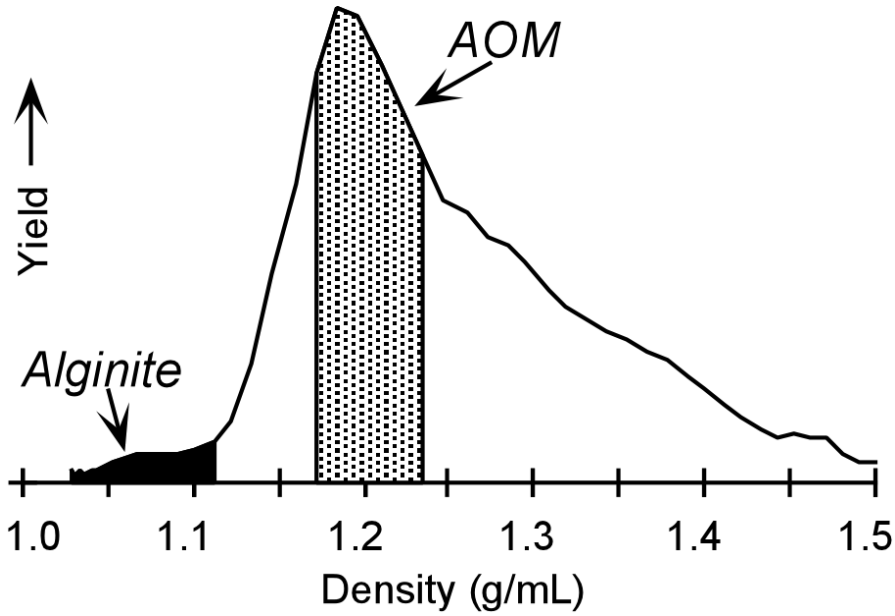

Infrared microspectroscopy. Powdered kerogen macerals (m < 0.5 mg) were placed between the two diamond windows (2mm diameter, 1 mm thickness) of a compression cell (7.5 cm X 5.1 cm, Spectra-Tech). After screw compression of the sample, the top window was removed. This preparation technique eliminates the problem of adsorbed water characteristic of KBr pellets and also minimizes spectrum distortion due to Christiansen effects[32,33]. A visible light 10X objective was used to select the area to be analyzed. Spectra were recorded from the sample placed on top of the bottom window. The micro FTIR analysis were performed on a Nicolet System 800 coupled with a Nic-Plan microscope which was fitted with a 250 μm narrow band MCT detector cooled to 77K. The standard analytical conditions were: 15X infrared objective, 40-60 μm diameter infrared spot, 32 scans, gain = 4, spectral resolution of 4 cm^{-1}. Spectra were ratioed to the background collected on a clean diamond window using the same analytical conditions.

All spectra presented in this paper are free from mathematical correction such as baseline correction or smoothing. The high quality of micro-infrared spectra allows mathematical treatments like second order derivative and Fourier deconvolution to be performed in order to resolve bands overlapping due to the large number of vibrations in the organic matter structure[34-37]. The assignments of the main I.R. bands were determined by reference to previous works[35,38-43]. In order to get more information concerning the components of the aliphatic region and particularly concerning methyl (CH_3-) and methylene (-CH_2-) groups, a Fourier self-deconvolution of the 2800-3000 cm-1 region was performed. This operation led to a better definition of the bands with reduction of the half-height width[34-37].

Confined pyrolysis in gold tubes. Measured aliquots (77-151 mg) of the alginite and AOM from the Toarcian kerogen were separately heated under argon in sealed gold tubes for 24 h at 70 MPa pressure at temperatures ranging from 250 to 375°C (Table 1). There was no 250°C experiment run on the alginite due to insufficient sample. The autoclaves and methods used for confined pyrolysis have been described previously[19,44]. After 24 hr, the tubes were quenched and removed from the autoclaves. They were pierced and gas contents determined by weight loss, after degassing overnight at 40°C. The tubes and their contents were extracted with $CHCl_3$ for 45 min. under reflux. The extracts were concentrated by rotary evaporation and deasphaltened with *n*-heptane. Saturated and aromatic hydrocarbons were separated from the deasphaltened extract by liquid chromatography (LC), eluting with CH_2Cl_2 on an alumina microcolumn. The polar fraction was eluted with CH_3OH. The saturates and aromatics were separated on a silica microcolumn, eluting with *n*-pentane and 2:1 *n*-pentane/CH_2Cl_2 respectively. The lowest temperature run of each maceral had low yields of extractable material (51 mg/g, Table 1). These two extracts were subjected to LC without deasphaltening to minimize losses during manipulation.

Table 1. Bulk geochemical data and molecular maturity parameters from artificial maturation experiments.

Sample	Temperature (°C)	Gas/ Initial OM (mg/g)	Extract/ Initial OM (mg/g)	Residue/ Initial OM (mg/g)	Satuates/ Initial OM (mg/g)	Aromatics/ Initial OM (mg/g)	Polars/ Initial OM (mg/g)	αβ/(βα+αβ) C_{30} Hopanes	αββ/(ααα+αββ) C_{29} Steranes	Triaro. Ster. Ratio[a]	TMN Ratio[b]
Alginite	300	34	51	898	4	9	37	0.62	0.21	0.18	0.41
Alginite	325	47	159	764	15	23	97	0.73	0.37	0.30	0.47
Alginite	350	101	611	89	53	119	237	0.89	0.54	0.79	0.51
Alginite	375	260	360	300	80	108	148	1.00	ND	1.00	0.58
AOM	250	31	51	901	1	5	45	0.54	0.24	0.12	0.43
AOM	300	71	294	572	12	47	105	0.74	0.33	0.15	0.46
AOM	325	94	408	436	20	71	155	0.86	0.49	0.31	0.48
AOM	350	130	359	420	33	96	143	0.90	0.53	0.78	0.50
AOM	375	215	225	439	39	87	85	ND	ND	1.00	0.58

ND — No hopanes or steranes detected.

(a) (C_{20} + C_{21}) / (C_{20} + C_{21} + C_{26} + C_{27} + C_{28}) triaromatic steroids

(b) Trimethylnaphthalene ("TMN") isomer ratio. (136-TMN + 137-TMN + 236-TMN) / (136-TMN + 137-TMN + 236-TMN + 146-TMN + 135-TMN + 127-TMN + 167-TMN + 126-TMN)[53]

Gas chromatography/mass spectrometry and flash pyrolysis. Analysis of the deasphaltened whole extracts and their saturate and aromatic fractions were performed using an HP 5890 Series II gas chromatograph with an HP 5972 Mass Selective Detector and a 60 m DB-5MS column (0.25 mm i.d., film thickness 0.1 μm). The column oven was operated under the following program: 40-130°C at 15 °/min., 130-300° at 3°/min. and then isothermal for 12 min. The on-column injector was temperature programmed to remain 3°C above the oven temperature. The MS was operated in selected ion mode at 1.1 scans/sec for saturates and 0.9 scans/sec. for aromatics and in full scan mode at 0.9 scans/sec for the whole extracts.

Flash pyrolysis of the extracted raw macerals and the extracted residues from the gold tubes was performed using an SGE Pyrojector II, coupled to the same GC/MS system described above, except that standard split injection was employed. The temperature program was isothermal for 5 min. at 40°C, then ramped 5°C/min. to 300°C and isothermally held for 15 min. The mass spectrometer was in full scan mode (50-550 daltons, 0.9 scans/sec., 70 eV ionization voltage). The Pyrojector furnace was held at a constant temperature of 620°C, with He carrier gas pressure maintained 30 kPa above that of the GC injector. A measured amount of sample (between 0.2 and 0.8 mg) was introduced into the furnace with a syringe designed for use with solids. Relative quantitations were performed using the mass spectral base peak of each compound of interest, then applying corrections based on appropriate MS response factors.

Analyses of the unheated whole kerogen and maceral concentrates (all pre-extracted with CH_2Cl_2) were also performed using a CDS 120 Pyroprobe, coupled to a HP 5890 gas chromatograph with a HP 5970 mass selective detector and a 25 m HP-1 column (0.2 mm i.d., film thickness 0.33 μm). A measured amount of each sample (≈1 mg) was pyrolyzed in a flow of helium for 20 sec in a platinum coil at 610°C, as measured by a thermocouple in the sample holder. The GC oven was operated under the following program: isothermal for 5 min. at 0°C; temperature programmed at 5°C/min. to 300°C and then isothermal for 15 min. The MS was operated in full scan mode (50-550 daltons, 0.86 scans/sec., 70eV ionization voltage).

It was found that the Py-GC/MS system with the CDS probe and 25 m HP-1 column fortuitously permitted the separation of methyl ketones from the normal hydrocarbons, so the resulting data are presented in the section on the unheated macerals. The Py-GC/MS dataset obtained using the SGE Pyrojector and 60 m DB-5MS column is more complete and is presented in the artificial maturation residue discussion. Flash pyrolysis-GC/MS and whole extract GC/MS peaks were identified based on mass spectra and GC retention indices, with reference to the Wiley and U. S. National Bureau of Standards computerized mass spectral libraries and the literature[45-53].

Evaluation of Separated Macerals

Bulk chemistry. The Rock Eval hydrogen index of the lamalginite concentrate (952 mg pyrolyzate/g C_{org}) is nearly double that of the AOM (573 mg/g C_{org}). The extraordinarily high value for the alginite indicates the potential for a nearly total conversion into gas and liquids. Its potential exceeds that of *Botryococcus*-related alginites isolated from non-marine torbanites[23]. The hydrogen index of the AOM, while still within the "oil-prone" range, shows a decrease from the value of 660 mg/g C_{org} observed for the whole kerogen, attributable to the removal of the alginite. Since this decrease is not major, it is likely that the character of the whole kerogen would be determined by its most abundant component (the AOM).

Transmission micro-FTIR spectroscopy provides further details of the nature of the two macerals. The aliphatic C-H stretching bands between 2800 and 3000 cm^{-1} strongly dominate the alginite spectrum (Figure 3a). The polymethylenic CH_2 rocking band at 720 cm^{-1} implies the presence of long aliphatic chains. The bands indicative of aliphatic CH_2 and CH_3 bending at about 1390-1460 cm^{-1} are also clearly recognizable, while the aromatic ring stretching band near 1600 cm^{-1} is barely discernible. The C=O (carbonyl and carboxyl) band near 1700 cm^{-1} is a sharp secondary feature of the spectrum.

The AOM spectrum also shows prominent aliphatic C-H stretching bands, as well as CH_2 and CH_3 bending (Figure 3b), however the polymethylenic CH_2 signature is absent. Aromatic ring stretching is clearly evident near 1600 cm^{-1} and aromatic C-H out-of-plane deformation in the 700-900 cm^{-1} region is a minor feature of the spectrum. The C=O band is also present, but is apparently relatively weaker than in the alginite spectrum.

The deconvolution results derived from the aliphatic C-H stretching region for the alginite (Figure 3c) show a clear predominance of the asymmetric and symmetric CH_2 bands. While the CH_2 bands are also prominent on the deconvoluted AOM spectrum (Figure 3d), the asymmetric CH_3 peak at 2956 cm^{-1} is relatively much stronger than on the alginite spectrum. This indicates a greater predominance of short- and branched-chain aliphatic carbon in the AOM, while the alginite is characterized by more long-chain aliphatic structures.

Figure 3. Transmission micro-FTIR spectra for the a) lamalginite and b) AOM separated from Lower Toarcian kerogen. Insets (c, d) show the results of deconvolution in the 2800-3000 cm^{-1} region.

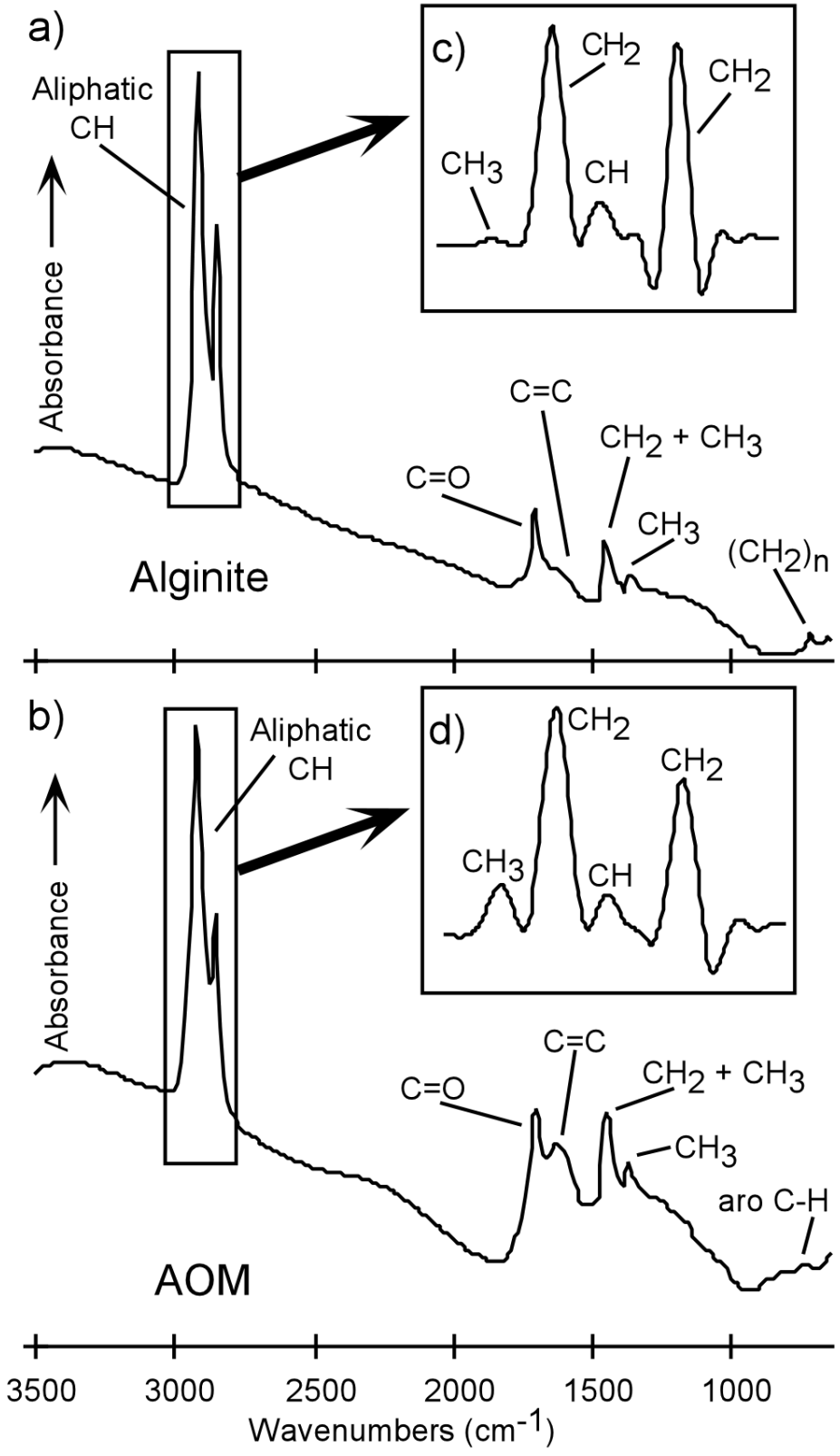

Molecular characterization. The flash pyrolyzate of the unheated, CH_2Cl_2-extracted alginite exhibits a strong predominance of *n*-alkenes and, secondarily, *n*-alkanes, with *n*-decene the most abundant (Figure 4a, Table 2). The most unusual feature of the pyrogram is the prominent series of mid-chain *n*-alkanones and *n*-alkenones. Aromatic hydrocarbons and heterocompounds are present in relatively minor amounts. An examination of the details of the C_{10}-C_{12} region of the pyrogram (Figure 4b) reveals that alkylbenzenes, alkylthiophenes, indenes and phenols are clearly discernible, yet are not significant components. At this scale, the minor series of *n*-alk-α,ω-dienes is apparent, as are the *n*-alkan-2-one and alken-2-one series. In the C_{20}-C_{21} *n*-alkane region of the alginite pyrogram (Figure 4c), the peaks due to the mid-chain *n*-alkanones and alkenones are the most prominent features. The *n*-alkanes and alkenes are still important compounds, while the dienes, alkan-2-ones and alken-2-ones are present in relatively minor quantities.

Mid-chain *n*-alkanones, with the general formula CH_3-$[CH_2]_n$-CO-$[CH_2]_m$-CH_3, have a characteristic mass spectral fragmentation pattern. They tend to produce paired ions arising from the cleavage of the bonds between the carbonyl carbon and either adjacent methylene carbon, yielding strong MS peaks corresponding to the CH_3-$[CH_2]_n$-CO^+ and CH_3-$[CH_2]_m$-CO^+ fragment ions[9,54-56]. For example, *n*-hexadecan-8-one produces relatively abundant m/z 127 and 141 fragment ions, corresponding to CH_3-$[CH_2]_6$-CO^+ and CH_3-$[CH_2]_7$-CO^+ respectively, while *n*-hexadecan-7-one produces more of the m/z 113 and 155 fragments (CH_3-$[CH_2]_5$-CO^+ and CH_3-$[CH_2]_8$-CO^+). Examination of the mass spectra of the mid-chain alkanones indicated in Figures 4a, 4c and 5a reveals that each Py-GC/MS peak is due to the coelution of several isomeric ketones, with their carbonyl carbons at the chain midpoint or within one or two carbons of it (Table 3). For example, the mass spectrum of the coeluting hexadecanones shows a predominance of both the *n*-alkan-7-one and the *n*-alkan-8-one, whereas the coeluting docosanones are for the most part a mixture of the *n*-alkan-10-one and *n*-alkan-11-one (Table 3). Other isomers with the carbonyl carbon farther from the chain midpoint are also present in relatively lesser amounts (Table 3). Thus the flash pyrolyzate of the alginite contains a complex mixture of *n*-alkanones that, with increasing carbon number, have chain lengths gradually increasing on both sides of a more or less central carbonyl group, rather than occurring as a simple homologous series.

The pyrogram of the unheated, CH_2Cl_2-extracted AOM also shows a predominance of normal hydrocarbons (Figure 4d), however their distribution differs significantly from that of the pyrolyzate of the alginite from the same kerogen (Figure 4a). In contrast to the alginite, no carbon number is favored, producing a distribution that is roughly equable and *n*-alkanes are more abundant relative to the *n*-alkenes. Prist-1-ene is found in relatively high concentration. Unlike the alginite case, alkylbenzenes and alkylthiophenes are major components of the AOM pyrolyzate (Figure 4d), seen more clearly in the detailed representation of the C_{10}-C_{12} region of the pyrogram (Figure 4e). Other aromatic hydrocarbons and thiophenic compounds

are also clearly discernible on the total ion current trace, including indenes, naphthalene and benzothiophene (Figure 4e). Phenol and C_1-C_3 alkylphenols are also present in relatively high concentrations. Alkan-2-ones are minor components, difficult to resolve chromatographically (Figure 4e). The mid-chain ketones are in very low relative concentrations, shown coeluting with other compounds on the detail of the C_{20}-C_{21} region of the total ion chromatogram (Figure 4f). The pyrogram of the whole kerogen closely resembles that of the AOM, consistent with the fact that the AOM is its majority constituent.

The C-2 and mid-chain ketones in the alginite pyrolyzate, each occurring as pairs of saturated and unsaturated compounds, are shown without the interference of coeluting compounds on the m/z 58 mass chromatogram (Figure 5a). Due to differences in mass spectral response factors, the mid-chain series appear less abundant, which is in fact not the case (Figure 4a). The m/z 58 data from the AOM pyrolyzate show essentially only the C-2 ketones (Figure 5b). Comparing Figures 5a, 5b, 4a and 4d, it is clear that the distinctive series of mid-chain ketones prominent in the alginite pyrolyzate is not a significant feature of the AOM.

Table 2. Py-GC/MS and GC/MS peak identification for Figures 4, 5, 7 and 9.

+ or +m	n-alkanes
Δ or Δm	*n*-alk-1-enes
◊ or ◊m	*n*-alk-α,ω-dienes
∇ or ∇m	*n*-alkan-2-ones
∇: or ∇:m	*n*-alken-2-ones
♦ or ♦m	mid-chain *n*-alkanones
♦: or ♦:m	mid-chain *n*-alkenones
Am	*n*-alkanoic acids
(where m is the carbon number)	
Hn	alkylcyclohexanes
Bn	alkylbenzenes
In	(alkyl)indenes
Nn	(alkyl)naphthalenes
Ψn	(alkyl)phenanthrenes
Φn	(alkyl)phenols
Θn	alkylthiophenes
BΘn	(alkyl)benzothiophenes
BΘBn	(alkyl)dibenzothiophenes
(where n is the extent of alkylation, e.g., 0 = none, 1 = methyl, 2 = dimethyl or ethyl)	
NPr	norpristane
Pr	pristane
Pr:	prist-1-ene
Ph	phytane
X	phthalate or silane contaminant

Figure 4. Py-GC/MS total ion current chromatograms. *Alginite*: a) C_7-C_{28} *n*-alkane range, b) details of the C_{10}-C_{12} *n*-alkane range and c) details of the C_{20}-C_{21} *n*-alkane range. *AOM*: d) C_7-C_{28} *n*-alkane range, e) details of the C_{10}-C_{12} *n*-alkane range and f) details of the C_{20}-C_{21} *n*-alkane range. See Table 2 for peak identification.

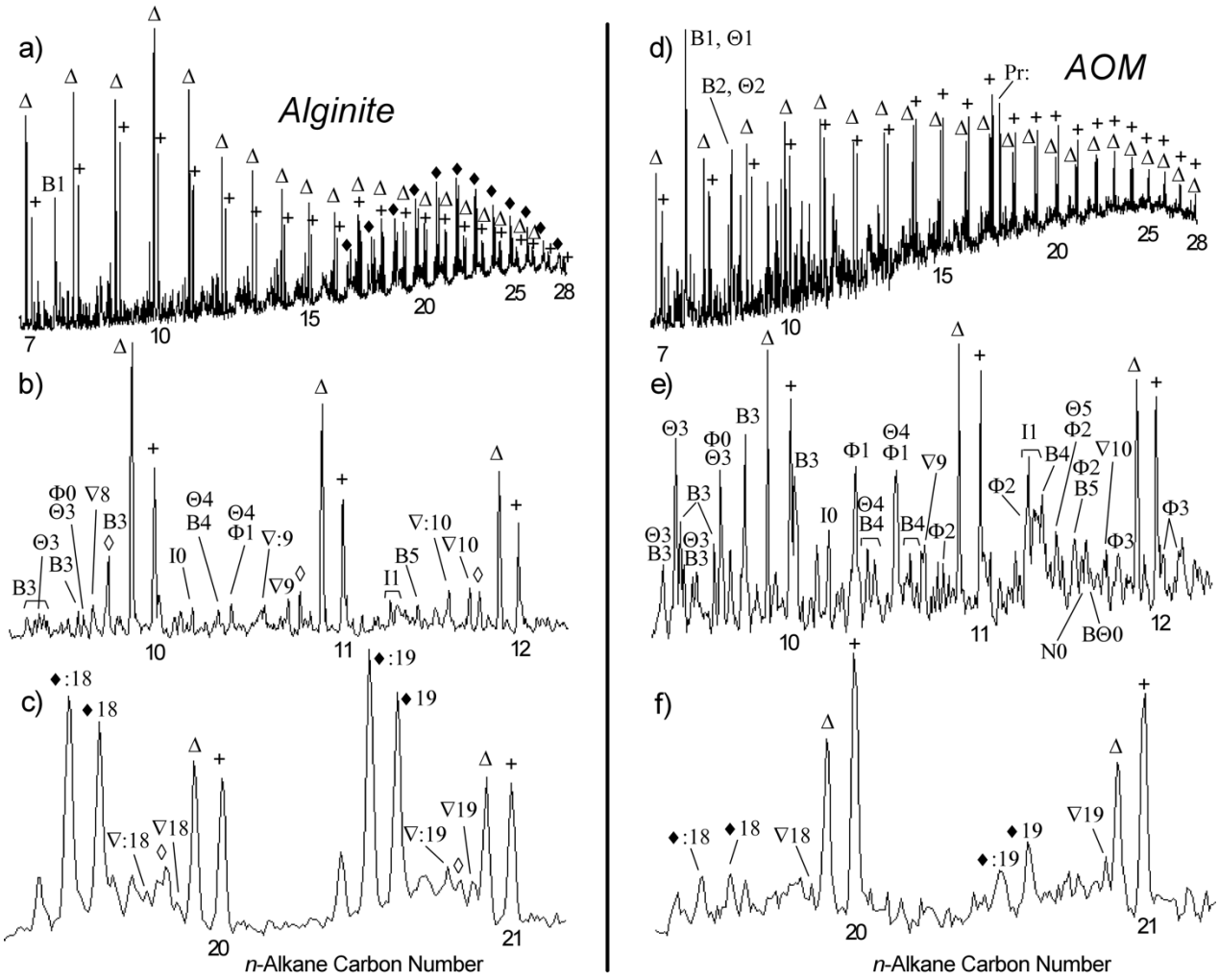

Table 3. Relative abundances of diagnostic mass spectral fragment ions produced by mid-chain *n*-alkanones with the indicated carbon numbers.

		C_{14}	C_{15}	C_{16}	C_{17}	C_{18}	C_{19}	C_{20}	C_{21}	C_{22}	C_{23}	C_{24}	C_{25}	C_{26}
ion	m/z	I (%)	I (%)	I (%)	I (%)	I (%)	I (%)	I (%)	I (%)	I (%)	I (%)	I (%)	I (%)	I (%)
$C_4H_7^+$	55	99	94	90	76	74	74	91	90	99	100	100	100	100
$C_4H_9^+$	57	94	100	100	100	100	100	100	100	100	77	72	64	57
$C_3H_6O^+$	58	100	95	98	76	72	72	72	76	58	54	44	30	31
$C_7H_{13}O^+$	113	***40***	***42***	***38***	26	21	11	12	12	12	11	10	8	8
$C_8H_{15}O^+$	127	***41***	***38***	***31***	***32***	***24***	***25***	18	16	16	12	14	10	12
$C_9H_{17}O^+$	141	29	***36***	***31***	***26***	***24***	***23***	***25***	15	15	10	9	10	10
$C_{10}H_{19}O^+$	155	15	19	***24***	***28***	***25***	***25***	***22***	***31***	18	17	13	11	12
$C_{11}H_{21}O^+$	169	8	10	13	17	***16***	***22***	***24***	***28***	***33***	***18***	19	15	9
$C_{12}H_{23}O^+$	183	5	10	8	8	13	***17***	***25***	***31***	***33***	***34***	***20***	***17***	***14***
$C_{13}H_{25}O^+$	197	0	0	7	5	5	7	10	14	18	***14***	***25***	12	13
$C_{14}H_{27}O^+$	211	0	0	3	5	6	5	5	7	10	14	14	13	11

Note: Each Py-GC/MS peak (Figures 4a, 5a) represents several coeluting mid-chain *n*-alkanone isomers. Principal diagnostic MS fragment ions are shown in italics. See text for further explanation.

Figure 5. Mass chromatograms (m/z 58) showing distributions of *n*-alkyl ketones in the flash pyrolyzates of a) alginite and b) AOM concentrates. See Table 2 for peak identification.

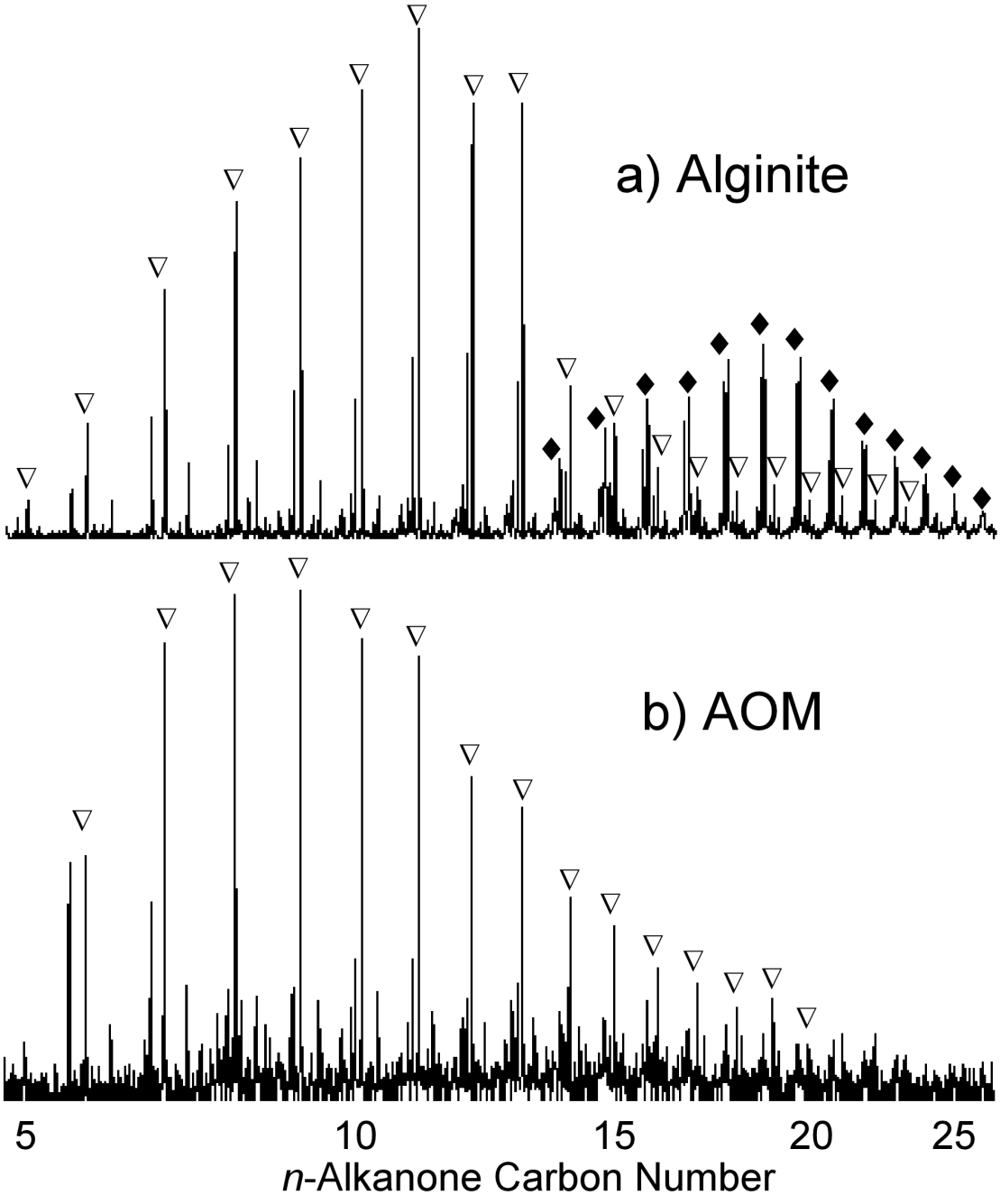

Artificial Maturation

Gas production. Gas yield is one of the important parameters monitored during the artificial maturation experiments conducted on the alginite and AOM concentrates. Gases likely included methane and other light hydrocarbons, as well as CO, CO_2, H_2O and H_2S (based on similar experiments done in this laboratory[57]), although gas composition was not determined in this study. Gas yields from the alginite remained low (<50 mg/g initial organic matter) at 300 and 325°C (Table 1, Figure 6a). They increased to 101 mg/g at 350°, then rose sharply to 260 mg/g at 375°C, probably due in part to secondary cracking of liquid products. In contrast, gas yields from the AOM increased steadily with increasing temperature from 31 mg/g at 250° to 215 mg/g at 375°, appearing consistently more gas prone than the alginite at every temperature step except the highest (Table 1, Figure 6a).

Solvent-extractable organic matter. The yields of $CHCl_3$-extractable material were relatively low (<160 mg/g initial organic matter) for the 300 and 325°C alginite experiments (Table 1, Figure 6b). By 350°, the yield increased markedly, reaching 611 mg/g. From this maximum, the yield declined to 360 mg/g at 375°. From a low point of 51 mg/g generated at 250°, the liquid yield from the AOM rises smoothly to a maximum of 408 mg/g at 325°, dropping gradually to 225 mg/g at 375°. The low, broad liquid generation curve of the AOM contrasts sharply with the steep, narrow alginite profile (Figure 6b). The maximum yield for the AOM is of lesser magnitude and occurs at a lower temperature than that of the alginite. The yields from the AOM are comparable to those produced by whole kerogen from other Lower Toarcian samples[58].

The amounts of the various LC fractions separated from the extracts also provide a means to monitor the progress of thermal alteration. Saturated hydrocarbons produced by the AOM increase gradually from 1 to 39 mg/g initial organic matter over the 250-375°C temperature range (Table 1). At 300 and 325°, the alginite produced less saturates than the AOM at the same temperatures, but yields increased sharply thereafter, such that at 375° the alginite produced 80 mg/g. Aromatic hydrocarbon yields from the AOM experiments increased steadily from 5 to 96 mg/g as temperatures were increased from 250 to 350° (Table 1). At 375°, yields decreased slightly to 87 mg/g. The alginite produced only minor amounts of aromatics at 300 and 325°, but yields jumped to 119 mg/g at 350° and diminished slightly at 375° to 108 mg/g. While the yields of saturates from the alginite are roughly double that of the AOM extracts produced at the two highest temperatures, aromatics are only about 25% more abundant (Table 1).

Yields of polar compounds from the AOM increase from 45 to a peak value of 155 mg/g at 325° and taper off at higher temperatures. Polar compound yields increase more rapidly for the alginite, attaining a maximum of 237 mg/g at 350° (Table 1), decreasing by 375°. The profiles of the polar compound generation curves closely parallel those of the whole extract (Table 1, Figure 6b), which is reasonable as the polars tend to be the majority constituents of the extract. The difference between

the total extract values and the sum of the saturate, aromatic and polar yields (Table 1) is ascribed to the asphaltenes, which were removed prior to LC separation. If the LC fraction data (Table 1) are recomputed as normalized percentages, the AOM extracts are consistently more aromatic than the alginite extracts produced at the same temperature, while the alginite products are relatively enriched in saturated hydrocarbons and polar compounds. Relative percentages of saturates and aromatics increase with temperature for both the alginite and AOM series, while polar percentages decline. The yields of saturates are likely increased at high temperature via secondary cracking of polar compounds and asphaltenes[59].

From the molecular perspective, the extracts from the artificial maturation experiments reflect the initial organic matter type. For example, the deasphaltened extract from the 325° alginite run exhibits a highly aliphatic character, showing a predominance of *n*-alkanes, in particular the even numbered homologues *n*-tetradecane and *n*-hexadecane (Figure 7a). There are subordinate series of *n*-alkanoic acids, *n*-alkan-2-ones and *n*-alkylcyclohexanes. Even the aromatic hydrocarbons and thiophenes have aliphatic character, witnessed by the minor series of *n*-alkylbenzenes and *n*-alkylthiophenes. Phenols, naphthalenes and benzothiophenes are detectable, but in very low relative concentrations.

The deasphaltened extract from the 325° AOM experiment also contains *n*-alkanes as major components, although the even predominance noted in the alginite extract is not present (Figure 7b). C_1-C_4 alkylbenzenes and alkylbenzothiophenes are important secondary components, as are C_2-C_3 alkylphenols. Larger polycyclic compounds, including phenanthrenes and dibenzothiophenes, are present in relatively minor amounts.

Hopane/moretane ratios for the alginite extracts increase smoothly from 0.62 to 1.00 over the 300-375°C temperature range (Figure 8a, Table 1). This parameter increases about the same rate for the AOM extracts, but values equivalent to those of the alginite extract are attained at temperatures approximately 25° lower (Figure 8a). By 350°, the rate of increase observed for the AOM extracts slows and the hopane/moretane ratio has about the same values as the 350° alginite extract. No hopanes were detected in the 375° AOM extract, even with single ion monitoring. The C_{29} $\alpha\beta\beta/(\alpha\alpha\alpha+\alpha\beta\beta)$ sterane ratio shows an effect similar to the hopane/moretane ratio (Table 1). At temperatures <350°, the extracts produced in the alginite experiments consistently have lower values of the ratio than do the AOM extracts produced at the same temperature.

In contrast to the saturate biomarker ratios, maturity indicators based on aromatic hydrocarbons show no significant dependence on organic matter type. For both the alginite and AOM, the triaromatic steroid ratios calculated on the extracts of the heating experiments increase steadily from around 0.15 to 1.00 with increasing temperatures (Figure 8b, Table 1). The trimethylnaphthalene ratios also behave similarly for both macerals, increasing from about 0.46 to 0.58 over the 325-375° range (Table 1).

Figure 6. Yields of a) gases, b) $CHCl_3$-extractable material and c) residue from artificial maturation experiments conducted on Toarcian alginite and AOM concentrates, reported as a mass fraction of the initial organic matter.

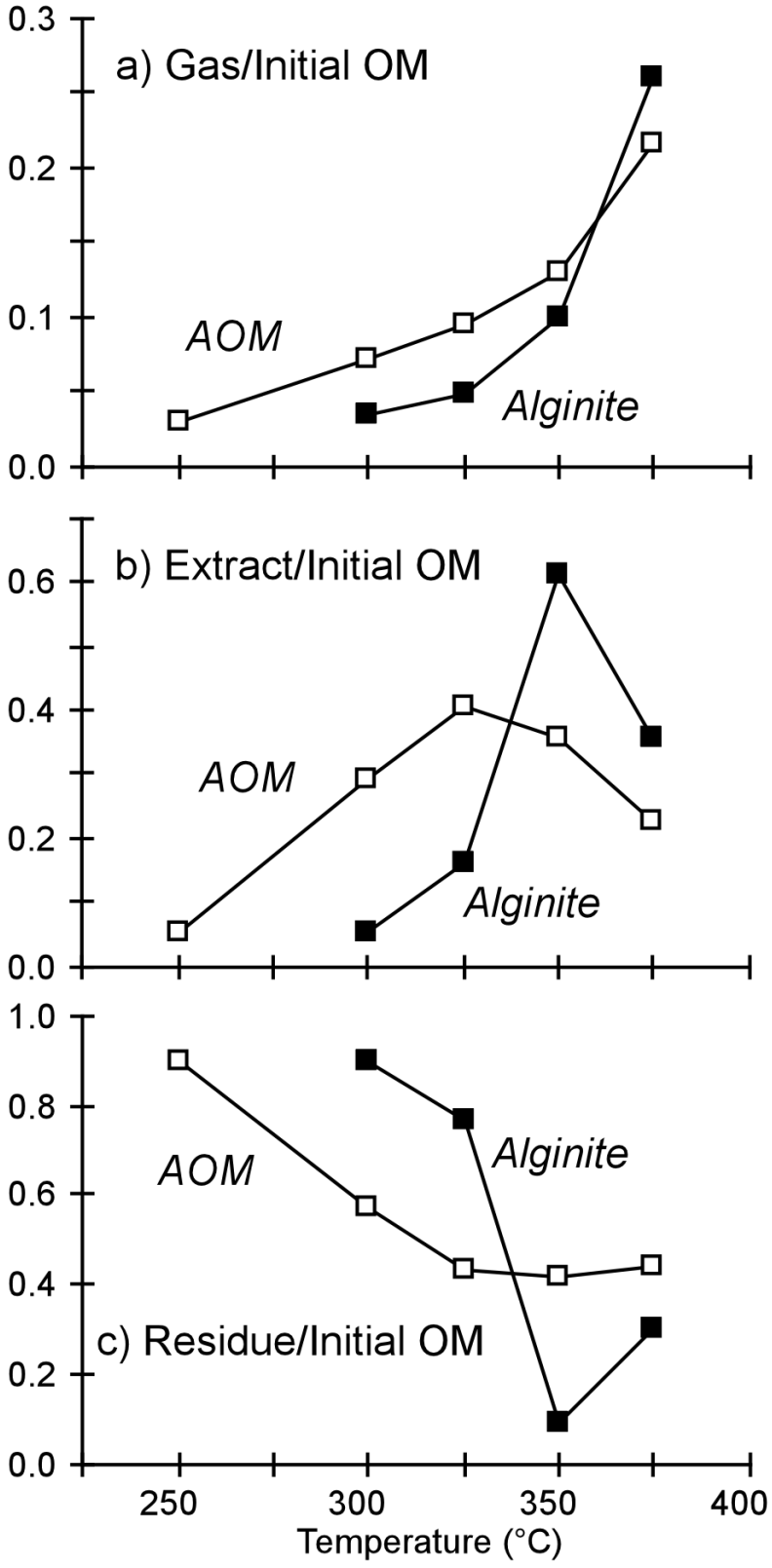

Figure 7. Partial GC/MS total ion current chromatograms of the deasphaltened $CHCl_3$ extracts of a) alginite and b) AOM after heating the macerals separately at 325°C and 70 MPa confining pressure for 24 h. See Table 2 for peak identification.

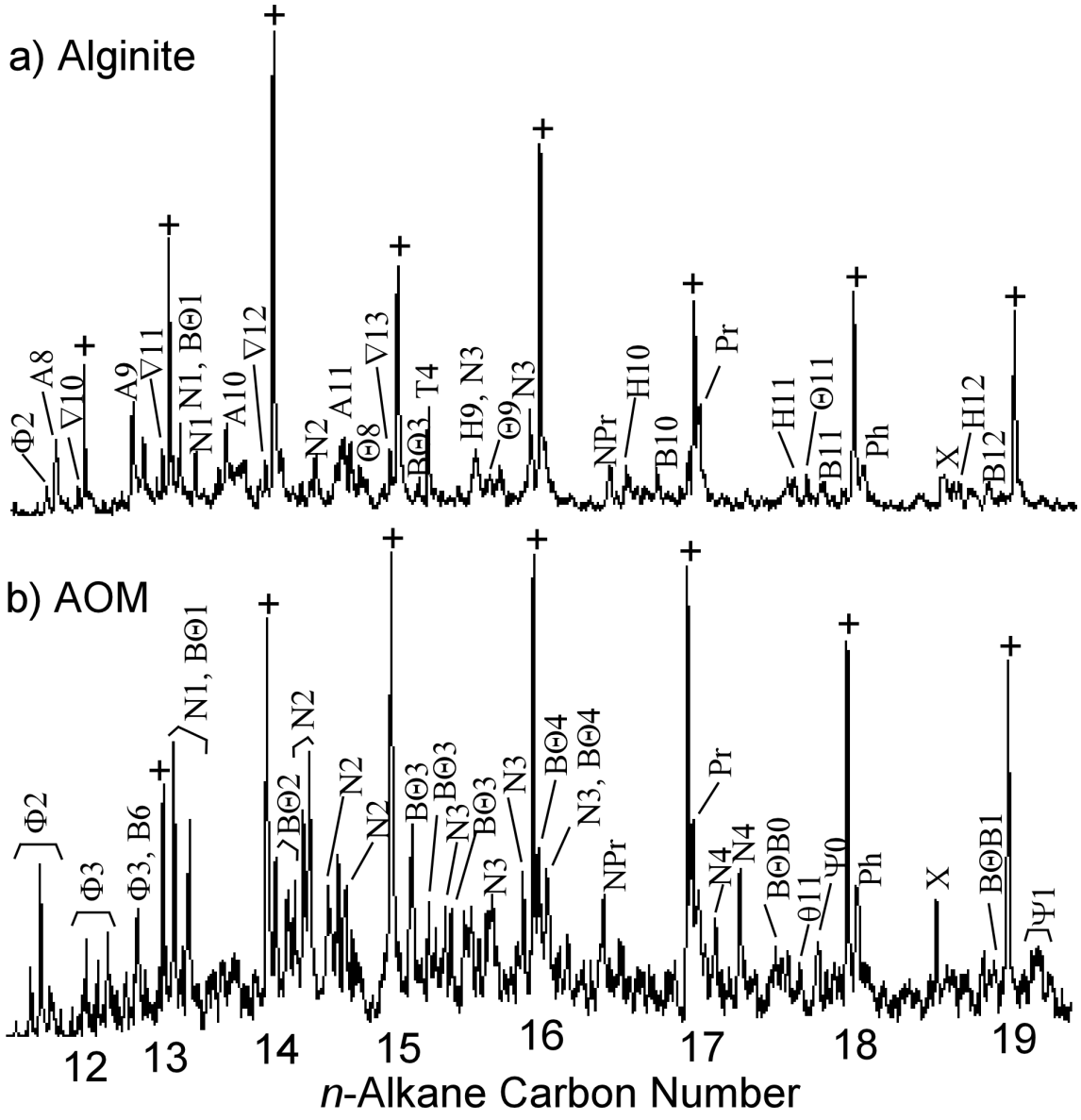

Figure 8. Molecular maturity parameters determined for the $CHCl_3$ extracts of the alginite and AOM concentrates after heating the macerals separately (70 MPa, 24 h) for the temperatures indicated.
a) $\alpha\beta/(\beta\alpha+\alpha\beta)$ C_{30} hopane ratios determined from m/z 191 mass chromatograms of the saturate fractions.
b) $(C_{20}+C_{21})/(C_{20}+C_{21}+C_{26}+C_{27}+C_{28})$ triaromatic steroid ratios determined from m/z 231 mass chromatograms of the aromatic fractions.

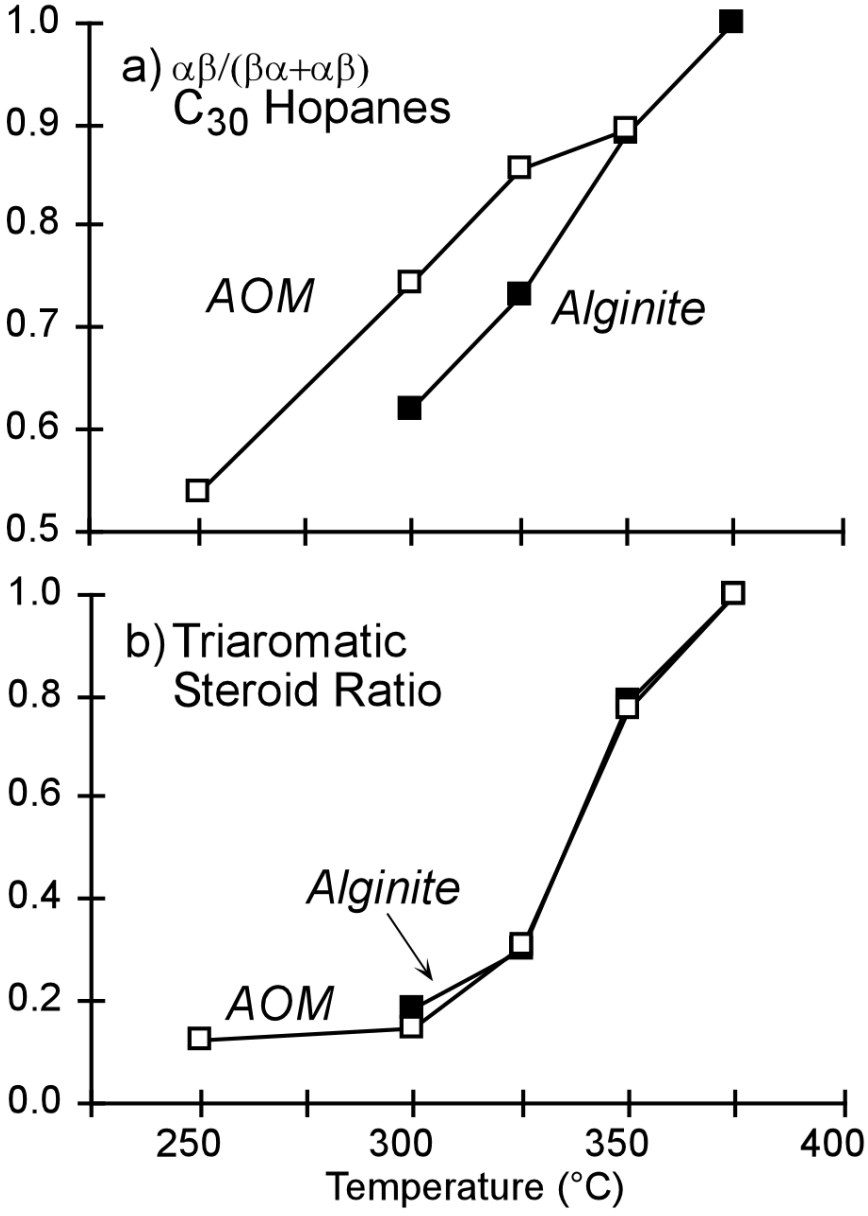

Residual organic matter. Amounts of organic residue from the alginite experiments after $CHCl_3$ extraction are relatively large (898 and 764 mg/g initial organic matter) after heating at 300 and 325°C (Table 1, Figure 6c). This indicates that little of the alginite reacted at these temperatures. However, at 350° the residue value of 89 mg/g demonstrates near total conversion of the original material. The increase in residue contents to 300 mg/g at 375° is evidence of polycondensation at this post-peak generation level. At 250° the AOM reacted only slightly, as 901 mg of residue per g of initial organic matter remains (Table 1, Figure 6c). By 325° the amount of residue is reduced to its minimum of roughly 400 mg/g, where it remains for the higher temperature runs. The near complete conversion of the original organic matter achieved by the alginite at its peak of generation was never realized by the AOM.

On the molecular level, an important feature of the unheated alginite concentrate was the high relative concentration of the mid-chain alkenones in its flash pyrolyzate (Figures 4a, 4c). We investigated the fate of alkanone moieties in the $CHCl_3$-extracted solid residues after artificial maturation by using flash Py-GC/MS. As representative examples, details of the C_{18} alkanone/C_{20} normal hydrocarbon region of the resulting pyrograms are shown in Figure 9a. After heating at 300°, the mid-chain alkyl ketones in the pyrogram of the residue are still strong, but have diminished slightly relative to the *n*-alkenes and alkanes, when compared with the raw alginite pyrogram in Figure 4c. At 325°, the ketones have diminished significantly. By the peak liquid generation temperature of 350°, ketones are no longer detectable, nor are the *n*-alkadienes. The *n*-alkene/alkane ratio also decreases gradually with increasing temperature. Examining the same region of the pyrograms for the AOM maturation series, no ketones are in evidence (Figure 9b). Rather there is a systematic increase in the relative abundance of methylphenanthrenes, attesting to the increasingly polyaromatic character of the residual material.

To invoke a more general view of the macromolecular structure of the maceral residues, it is apparent from Figure 4 that, aside from the ketones, the most important pyrolysis products of the unheated macerals are the normal alkanes and alkenes, the benzenes, the thiophenes and the phenols. A ternary diagram summarizes the shifts in relative concentrations of the aliphatics, aromatics and heterocompounds in the residue flash pyrolyzates as a function of artificial maturation temperature (Figure 10). (It is important to remember that the temperatures cited throughout this discussion refer the conditions of the day-long confined heating in gold tubes, not the flash pyrolysis temperature which was always 610-620°.)

The residue from the 250°C AOM heating experiment shows little evidence of change from the raw, unheated maceral (Figure 10). As temperatures increase to the peak liquid generating temperature of 325°, there is a progressive decrease in the relative percentage of alkylthiophenes and phenols in the flash pyrolyzate of the residue, but little change in the aliphatic/aromatic ratio. Relative thiophene concentrations diminish at a greater rate at lower temperatures, whereas preferential loss of phenols was noted at higher temperatures. Above 325°, the main change in

the residue is increasing aromaticity, the rate of which accelerates between 350 and 375° (Figure 10). The shape of the alginite maturation profile in Figure 10 roughly resembles that of the AOM, but the curve is significantly shifted towards the aliphatic pole of the diagram. One key difference is that the alginite pyrolyzate, already relatively low in thiophenes and phenols (Figure 4), shows little loss of these components at temperatures ≤325° (Figure 10). Instead the predominant alteration is the increasing relative importance of aliphatic hydrocarbons. The residue at the peak liquid generation temperature of 350° displays a virtually complete loss of the heterocompounds, whereas by 375° a significant increase in aromaticity is evident.

Figure 9. Partial Py-GC/MS total ion current chromatograms (*n*-eicosane region) of the $CHCl_3$ extraction residues after heating the a) alginite and b) AOM separately for the temperatures indicated (70 MPa, 24 h). See Table 2 for peak identification.

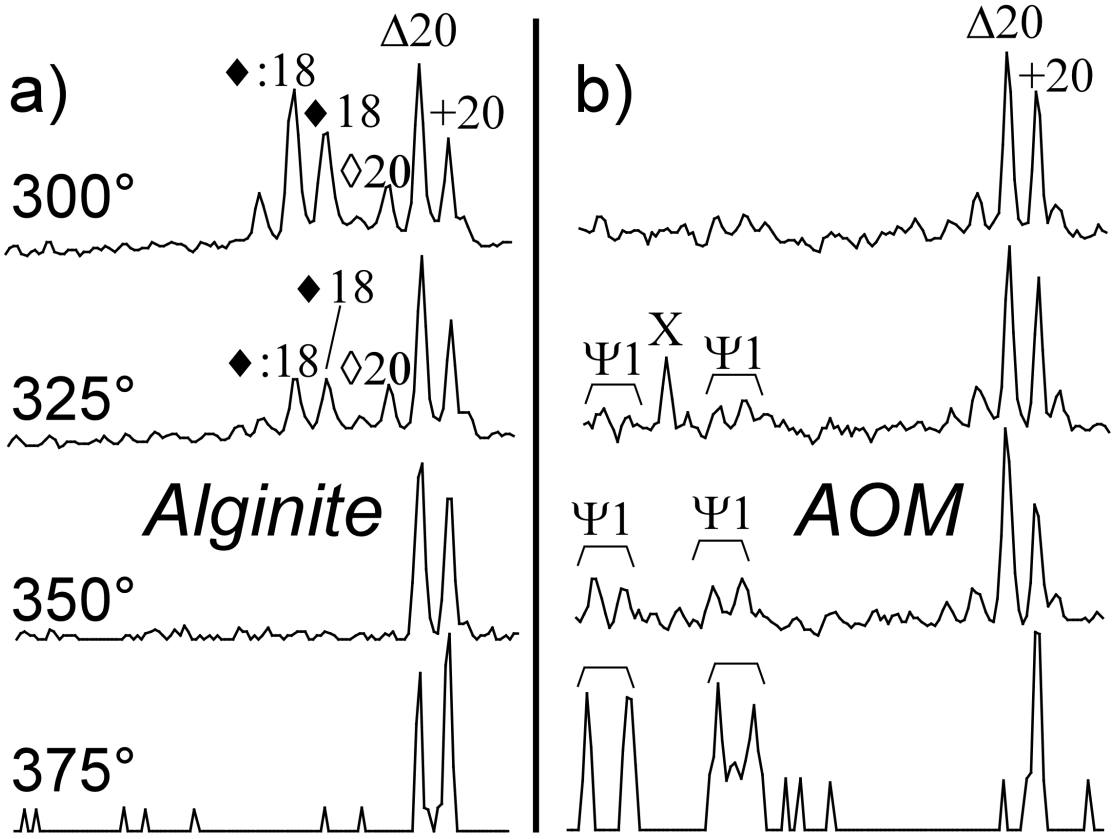

Figure 10. Ternary diagram comparing relative concentrations of aliphatic hydrocarbons (C_8-C_{29} *n*-alkanes and *n*-alkenes), aromatic hydrocarbons (C_1-C_4 alkylbenzenes, C_0-C_3 (alkyl)naphthalenes, (alkyl)phenanthrenes and (alkyl)anthracenes), and heterocompounds (C_1-C_4 alkylthiophenes, C_0-C_3 (alkyl)phenols) from the flash pyrolyzates of the $CHCl_3$ extraction residues after heating the maceral concentrates separately for the temperatures indicated (70 MPa, 24 h). Quantitations were performed on mass chromatograms of the base peaks of the individual compounds and were corrected by appropriate mass spectral response factors.

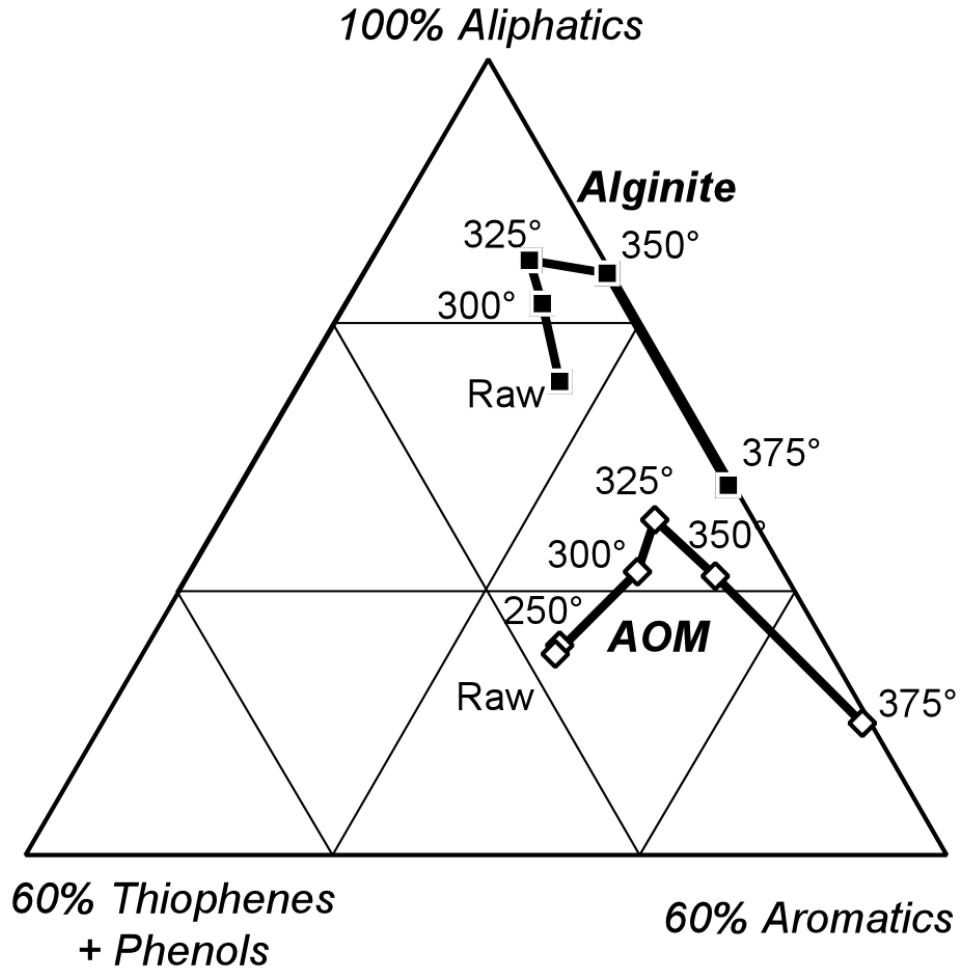

Discussion and Conclusions

Insights into kerogen structure and formation. The Rock Eval, FTIR and Py-GC/MS analyses indicate that the dull yellowish-orange fluorescing AOM is oil-prone and predominantly aliphatic in character. The nature of this Lower Toarcian Type II kerogen sample is largely dictated by the character of the AOM, which is the major component (60% by volume). What was unexpected, however, was the nature of the bright yellow fluorescing lamalginite, the details of which remained obscure during studies of the whole kerogen, as it is only accounts for 20% of the total volume. Taken in isolation, the alginite is two-thirds more oil prone than its co-occurring AOM, as measured by Rock Eval. The alginite is correspondingly more aliphatic than the AOM and the aromatic, thiophenic and phenolic moieties are relatively much less important (Figures 3, 4). This is consistently clear from all analytical techniques employed in this study. It is evident that the alginite concentrate is chemically distinct from its companion AOM in this kerogen and that the full extent of its uniqueness would not have been revealed without the density separation step.

Our previous attempt to isolate the alginite from another sample of the Lower Toarcian kerogen of the Paris Basin[60] was not very successful. In that experiment, the alginite concentrate obtained was only 70% pure. In retrospect, it is evident that we began with insufficient sample for optimum separation and selected too high a density (1.15 g/mL) for a clean alginite fraction. Another difficulty was that the previous Toarcian kerogen sample only contained 10% alginite by volume, compared with 20% in the present study. The resulting pyrograms[60] showed only minor differences between alginite and AOM concentrates, with no evidence of ketones in the alginite pyrolyzates.

With results from all the analytical techniques in agreement that the alginite isolated for the present study is chemically distinctive, it remains to assess what insights have been gained into the origin of the Lower Toarcian kerogen and its macerals. The FTIR and flash pyrolysis results indicate that the alginite is extremely aliphatic, but most remarkably, its flash pyrolyzate contains several series of mid-chain ketones in high relative abundance (Figures 4a, 4c, 5a), a feature neither observed in the pyrolyzates of the AOM (Figures 4d, 4f, 5b) nor the whole kerogen. Mid-chain ketones have been recognized previously in the flash pyrolyzates of a Coorongite[54], which is in effect a natural concentrate of the resistant biopolymer algaenans derived from the extant, thick-walled lacustrine green alga *Botryococcus braunii*. Mid-chain ketones were also reported from an immature Tertiary lacustrine kerogen rich in *Botryococcus*[51].

The pyrolyzates of algaenans prepared from extant marine eustigmatophytes of the genus *Nannochloropsis* also contain abundant mid-chain ketones[9], whose distribution bears strong similarities with those in the Toarcian alginite pyrolyzate (Figures 4a, 5a). One difference is the ketone carbon number range: C_{16}-C_{26} with a C_{19} maximum (Figure 5a) compared to C_{20}-C_{34} with a maximum at C_{30} for

Nannochloropsis[9]. As with the *Nannochloropsis* pyrolyzate, there is a subordinate series of *n*-alkan-2-ones produced from the Toarcian alginite. To our knowledge, the Toarcian alginite discussed herein is the only example of ancient marine organic matter whose pyrolyzate contains mid-chain alkanones in such high relative concentrations. While the paleobiology of the eustigmatophytes is unknown[61], the chemical similarity of the Toarcian alginite to the *Nannochloropsis* algaenans tempts us to suggest that our sample might possibly be the fossilized remains of an Early Mesozoic thin-walled planktonic alga resembling or ancestral to the eustigmatophytes. A chlorophyte origin for the algal remains in other Lower Toarcian kerogens was previously proposed on the basis of alkylnitrile content in their pyrolyzates[8].

A closer examination of the Toarcian alginite pyrolyzate's mid-chain ketones reveals the lack of a constant alkyl chain length on either side of the carbonyl group (Table 3). In contrast, the Recent *Nannochloropsis* algaenans produced homologous series of *n*-alkan-17-ones and *n*-alkan-18-ones upon pyrolysis[9] and the *Botryococcus* produced *n*-alkan-9-ones and *n*-alkan-10-ones[52,54]. In the latter cases, the authors interpret the alkanones in the pyrolyzates to imply ether bridges cross-linking the alkyl chains at constant distances from the ends of the chains. In the case of the Toarcian marine alginite, the site of cross-linking is apparently more variable. A comparison of the *Nannochloropsis* and *Botryococcus* data also suggests that the position of cross-linking may also be exploited as a chemotaxonomic feature. At this level of detail, the Toarcian alginite is clearly distinctive; it may derive from an alga with variable siting of cross-links or perhaps represents a mixture of several algal species. We were not able to resolve this uncertainty by petrographic means, due to the alginite particles' small size and lack of distinctive morphology (Figure 1).

It must also be considered that the presence of the mid-chain ketones in alginite pyrolyzates may be due to selective oxidation of algal lipids at about the time of sedimentation, reflecting the conditions of the particular depositional environment and a complex preservation pathway, rather than direct derivation from algal biopolymers[62]. The oxidized Coorongite contains relatively abundant ketones in its pyrolyzate[54], while the algaenan produced in the laboratory from fresh *Botryococcus braunii* does not[63]. In any event, the presence of the ketones is unlikely to be an artifact of the sample preparation procedure used in the present study, as other alginites isolated by density separation from both marine[16] and lacustrine kerogens[23,27] did not produce them upon pyrolysis.

The origin of the AOM is also a topic which merits discussion, especially as it is the majority constituent of this Toarcian kerogen sample and its significantly aliphatic character reveals that it is oil-prone in its own right (Figures 3, 4). The significant chemical differences between the AOM and its companion alginite, particularly as demonstrated by flash pyrolysis (Figures 4, 5), suggest that the resistant algal biopolymer made little direct contribution to the AOM. The presence of important aromatic and phenolic moieties in the AOM pyrolyzate (in addition to the aliphatic) implies more heterogeneous organic matter sources, which likely

included bacterial biomass[64] and algal lipids[11]. The greater preponderance of CH_3 bands relative to CH_2 in the micro-FTIR results for the AOM (Figure 3) implies relatively more branched aliphatic chains, which might indicate a bacterial contribution[8,65,66]. The minor vitrinite contamination in this AOM concentrate would also be a source some of the phenols and alkylbenzenes in the pyrolyzate[53]. The relatively abundant alkylthiophenes (Figure 4e) suggests extensive thioether cross-linking formed during early diagenetic sulfurization[67], implying radically different formation pathways for the AOM and alginite macerals, even though they are the components of a single kerogen sample, much like that previously observed in Type II-S kerogen macerals[16].

Implications for petroleum generation. The behavior of the alginite during artificial maturation differs markedly from that of the AOM (Table 1, Figures 6-10). The alginite escaped significant thermal degradation until the 350°C temperature level, at which point its conversion was nearly total. In contrast to this abrupt, relatively late transformation, the AOM isolated from the same kerogen sample underwent a more gradual conversion as temperatures were increased, reaching peak generation at only 325°C. The nature of the extractable material produced is also different — more aromatic and thiophenic in the case of the AOM, while the alginite products are relatively enriched in saturated hydrocarbons and polar compounds (Table 1, Figure 7).

Differences in the thermal responses of the alginite and AOM can be related to their composite activation energies and ultimately to their biological precursors and early diagenetic history. The gradual thermal transformation experienced by the AOM implies compositional heterogeneity and a broad distribution of activation energies, akin to that previously determined for whole Lower Toarcian and similar kerogens[68,69]. In contrast the nearly total, high-temperature conversion of the alginite indicates compositional homogeneity and a narrow range of activation energies of relatively high magnitude, in accord with estimates based on microfluorimetric properties of the various liptinite macerals[70] and like that determined for Type I (algal-dominated) kerogen[68,69].

In a companion study, we performed artificial maturation experiments on alginite and organic groundmass isolated from two torbanites using the same procedures outlined in this article[23]. These lacustrine, *Botryococcus*-related alginites also produced abundant yields of solvent-extractable material at their peak generation stage, in amounts comparable to the Toarcian alginite. However, they required greater thermal stimulation to achieve this[23], peaking at 375°C compared to 350°C in the Toarcian case (Table 1, Figure 6b). Like the Toarcian AOM, the heterogeneous groundmass concentrates from the lacustrine samples displayed broad generation curves and attained their maximum extract yields at a lower temperature than their co-occurring alginites[23]. But this maximum (occurring at 350°C) was at a higher temperature than the 325°C level observed for the Toarcian AOM (Table 1, Figure 6b). The maximum extract yields for the lacustrine organic groundmass samples (ca. 250 mg/g initial organic matter) were also significantly lower than the 408 mg/g

achieved by the marine AOM (Table 1), reflecting their lower generation potential predicted by Rock Eval hydrogen indices[23] and different organic matter sources.

While the lacustrine alginite flash pyrolyzates contained an overwhelming predominance of normal hydrocarbons[23], they lacked the *n*-alkyl ketones observed in the marine alginite (Figure 4a). These ketones imply abundant ether cross-linkages in the Toarcian alginite, the thermolytic cleavage of which permits lower temperature depolymerization, while higher energy C-C bonds evidently must be broken in the case of the lacustrine alginites, requiring somewhat higher temperatures. The role of the ether linkages in hydrocarbon generation from the Toarcian alginite is demonstrated by the diminution and ultimate disappearance of the alkyl ketones in the flash pyrolyzates of the residues from the artificial maturation experiments, as the maximum generation level is attained at 350°C (Figure 9a) and the ether bridges are destroyed.

Like the organic groundmass found in the torbanites, the Toarcian AOM is heterogeneous and partly degraded. However, its pyrolyzate is clearly distinguished from those of the torbanite groundmass by its high relative concentrations of thiophenic sulfur. Cleavage of the relatively labile C-S bonds during artificial maturation evidently permits the Toarcian AOM to achieve its peak generation at only 325°C (Figure 6b), lower than the torbanite groundmass, the thiophenic sulfur content of which was insignificant[23]. There is also a relative sulfur enrichment in the Toarcian AOM compared to its companion alginite (Figures 4b, 4e), which contributes to its lower temperature for peak liquid generation (Figure 6b). Examination of the flash pyrolyzates of the AOM residues from the artificial maturation experiments reveals a drop in the relative concentration of heteroatomic moieties, in particular the alkylthiophenes, as the peak generation temperature of 325°C is approached (Figure 10), implying an important role for the sulfur in this "early generation" phenomenon. While this behavior has previously been observed for high sulfur *whole* kerogen[68,69], we observe it here for the kerogen *component* relatively most enriched in sulfur. As a secondary effect, the relatively lower temperature release of sulfur-bound biomarkers[71] could explain the more rapid increase in biomarker ratios observed for the AOM (Table 1, Figure 8a).

In nature, petroleum generated from a kerogen would be a mixture of the liquids produced by each of its components, in a blend that would change as thermal alteration progressed, as the various constituents each reached their window of generation. The overall generation profile would be the proportional sum of the reaction progress curves for the decomposition of the individual components. In the case of the Toarcian kerogen sample, the AOM is the majority constituent and would have the greatest influence on slope and amplitude of the generation curve. The secondary components of this kerogen — alginite, vitrinite and inertinite — would also have an effect. Since we have demonstrated that the generation potential of the alginite is so much greater than that of the AOM, it would have a proportionately larger impact on the overall profile. In view of the low petroleum potential presumed for vitrinite and especially inertinite[21], the net effect of these latter two macerals

would be to depress the overall generation yield (when presented as proportional to the weight of the total initial organic matter). As demonstrated by the results of this study and its companion project[23], a multi-component model of kerogen composition can serve to improve predictions of oil generation from kerogens and related source rocks in sedimentary basins.

Acknowledgments. The authors gratefully acknowledge financial support from CREGU, Centre National de la Recherche Scientifique and Southern Illinois University, without which this work would not have been possible. We would also like to thank J. Crelling, Z. Han, C. Thies, B. Poty, S. Ashkan, R. Michels, L. Mansuy and all the staff at CREGU for their assistance throughout the duration of the project. We acknowledge the helpful discussions with C. Largeau and F. Gelin, as well as the comments of an anonymous reviewer.

References

(1) Landais, P.; Rochdi, A.; Largeau, C.; Derenne, S. *Geochim. Cosmochim. Acta* **1993**, *57*, 2529-2539.

(2) Stout, S. A. *Int. J. Coal Geol.* **1993**, *24*, 309-331.

(3) Teichmuller, M. *Org. Geochem.* **1986**, 10, 581-599.

(4) Largeau, C.; Derenne, S.; Casadevall ,E.; Kadouri, A.; Metzger, P. *Org. Geochem*. **1984**, *6*, 327-332.

(5) Largeau, C.; Derenne, S.; Casadevall, E.; Kadouri, A.; Sellier, N. *Org. Geochem*. **1986**, *10*, 1023-1032.

(6) Tegelaar, E. W.; de Leeuw, J. W.; Derenne, S.; Largeau, C. *Geochim. Cosmochim. Acta* **1989**, *53*, 3103-3106.

(7) Derenne, S.; Largeau, C.; Berkaloff, C.; Rousseau, B.; Wilhelm, C.; Hatcher, P. G. *Phytochem*. **1992**, *31*, 1923-1929.

(8) Derenne, S.; Le Berre, F.; Largeau, C.; Hatcher, P. G. ; Connan, J.; Raynaud, J. F. *Org. Geochem.* **1992**, *19*, 345-350.

(9) Gelin, F.; Boogers, I.; Noordeloos, A. A. M.; Sinninghe Damsté, J. S.; Hatcher, P. G.; de Leeuw, J. W. *Geochim. Cosmochim. Acta* **1996***, 60*, 1275-1280.

(10) Gelin, F.; Boogers, I.; Noordeloos, A. A. M.; Sinninghe Damsté, J. S.; Riegman, R. G.; de Leeuw, J. W. In, *Isolation and chemical characterization of resistant macromolecular constituents in microalgae and marine sediments.* Gelin, F., Ph.D. thesis, University of Utrecht. Geologica Ultraiectina No. 139, 1996, pp 59-79.

(11) Boussafir, M.; Gelin, F.; Lallier-Vergès, E.; Derenne, S.; Bertrand, P.; Largeau, C. *Geochim. Cosmochim. Acta* **1995,** *59*, 3731-3747.

(12) Gelin, F.; Sinninghe Damsté, J. S.; Harrison ,W. N.; Maxwell, J. R.; de Leeuw, J. W. *Org. Geochem.* **1995***, 23*, 555-566.

(13) Kruge, M. A.; Crelling, J. C.; Rimmer, S. M. In *1988 Eastern Oil Shale Symposium;* Lazar, D. J., Ed.; Institute for Mining and Minerals Research: Lexington, KY, USA., 1989, pp 411-417.

(14) Stankiewicz, B. A.; Kruge, M. A.; Crelling, J. C.; Salmon, G. L. *Energy Fuels.* **1994**, *8*, 1513-1521.

(15) Hartgers, W. A.; Sinninghe Damsté, J. S.; de Leeuw, J. W.; Ling, Y.; Crelling, J. C. *Org. Geochem.* **1995**, *23*, 777-784.

(16) Stankiewicz, B. A.; Kruge, M. A.; Mastalerz, M.; Salmon, G. L. *Org. Geochem.* **1996**, *24*, 495-509.

(17) Lewan, M.D. *Phil. Trans. R. Soc. Lond. A* **1985**, *315*, 123-134.

(18) Saxby J. D.; Bennett A. J. R.; Corcoran J. F.; Lambert D. E.; Riley K. W. *Org. Geochem.* **1986**, *9*, 69-81.

(19) Landais, P.; Michels, R.; Poty, B.; Monthioux, M. *J. Appl. Anal. Pyrol.* **1989**, *16*, 103-115.

(20) Landais, P.; Muller, J.-F.; Michels, R.; Oudin, J.-L.; Zaugg, P. *Fuel* **1989**, *68*, 1616-1619.

(21) Landais, P.; Zaugg, P.; Monin, J.-C.; Kister, J.; Muller, J. F. *Bull Soc. géol. France* **1991**, *162*, 211-217.

(22) Kruge, M. A.; Landais, P. *Amer. Chem. Soc. Div. Fuel Chem. Prepr.* **1992**, *37* (4), 1595-1600.

(23) Kruge, M. A.; Landais, P.; Bensley, D. F. *Organic Geochemistry* **1996**, 24, 737-750.

(24) Tissot, B.; Welte, D. H. *Petroleum Formation and Occurrence*, 2nd ed. Springer-Verlag: Berlin, 1984, 699 p.

(25) Espitalié, J.; Laporte, J. L.; Madec, M.; Marquis, F.; Leplat, P.; Paulet, J.; Boutefeu, A. *Rev. Inst. Fr. Pét.* **1977,** *32*, 23-42.

(26) Bensley, D. F.; Crelling, J. C. *Fuel* **1994**, *73*, 1306-1316.

(27) Han, Z.; Kruge, M. A.; Crelling, J. C.; Stankiewicz, B. A. *Org. Geochem.* **1995**, *21*, 39-50.

(28) Dyrkacz, G. R.; Horwitz, E. P. *Fuel* **1982**, *61*, 3-12.

(29) Dyrkacz, G. R.; Bloomquist, C. A. A.; Ruscic, L. *Fuel* **1984**, *63*, 1367-1374.

(30) Dyrkacz, G. R.; Bloomquist, C. A. A.; Ruscic, L.; Crelling, J. C. *Energy Fuels* **1991**, *5*, 155-163.

(31) Crelling, J. C. *Am. Chem. Soc. Div. Fuel Chem. Prepr.* **1989**, *34* (1), 249-255.

(32) Ruau, O.; Mansuy, L.; Landais, P. *C. R. Acad. Sci. Paris* **1995**, *321* (Serie IIa), 201-208.

(33) Ruau, O.; Landais, P.; Gardette, J. L. *Fuel* **1997** (in press).

(34) Kauppinen, J. K.; Moffatt, D. J.; Mantsch, H. H.; Cameron D. G. *Anal. Chem.* **1981**, *53*, 1454-1457.

(35) Wang, S. H.; Griffith, P. R. *Fuel* **1985**, *64*, 229-236.

(36) Davis, R.A.; White, R. L. *Anal. Chem.* **1989**, *61*, 33-37.

(37) Pierce, J.A.; Jackson, R.S.; Van Every, K.W.; Griffiths, P.R.; Hongjin, G. *Anal. Chem.*, **1990**, *62*, 477-484.

(38) Williams, D.H.; Fleming, I. *Spectroscopic methods in organic chemistry*; McGraw-Hill: London, 1966, pp 41-76.

(39) Bellamy, L. J. (1975) *The infrared spectra of complex molecules*; 3rd Ed., Chapman and Hall, Ltd.: London; 433 p.

(40) Robin, P. L.; Rouxhet, P. G.; Durand, B. In *Advances in Organic Geochemistry*; Campos, R.; Goni, J., Eds.; Enadisma: Madrid, 1977, pp 693-716.

(41) Painter, P.C.; Snyder, R. W.; Starsinic, M.; Coleman, M. M.; Kuehn, D. W.; Davis, A. *Appl. Spectroscopy* **1981**, *35*, 475-485.

(42) Guiliano, M.; Mille, G.; Doumenq, P.; Kister, J.; Muller, J. F. In *New Advanced Methodologies in Coal Characterization*. *Coal Science and Technology, Vol. 15*, Charcosset, H., Ed.; Elsevier: Amsterdam, 1990; pp 399-416.

(43) Landais, P.; Rochdi, A. *Fuel*, **1993**, *72*, 1393-1401.

(44) Monthioux M., Landais P.; Monin J.-C. *Org. Geochem.* **1985**, *8*, 275-292.

(45) Radke, M.; Garrigues, P.; Willsch, H. *Org. Geochem.* **1990**, *15*, 17-34.

(46) Douglas, A. G.; Sinninghe Damsté, J. S.; Fowler, M. G.; Eglinton, T. I.; de Leeuw, J. W.*Geochim. Cosmochim. Acta* **1991,** *55*, 275-291.

(47) Eglinton, T. I.; Sinninghe Damsté, J. S.; Pool, W.; de Leeuw, J. W.; Eijkel, G.; Boon, J. J. *Geochim. Cosmochim. Acta* **1992,** *56*, 1545-1560.

(48) Hartgers, W. A.; Sinninghe Damsté, J. S.; de Leeuw, J. W. *J. Chromatogr.* **1992**, *606*, 211-220.

(49) Nip, M.; de Leeuw, J. W.; Schenck, P. A. *Geochim. Cosmochim. Acta* **1988**, *52*, 637-648.

(50) Nip, M.; de Leeuw, J. W.; Crelling, J. C. *Energy & Fuels* **1992**, *6*, 125-136.

(51) Sinninghe Damsté, J. S.; de las Heras, F. X. C.; de Leeuw, J. W. *J. Chromatogr.* **1992,** *607*, 361-376.

(52) Sinninghe Damsté, J. S.; de las Heras, F. X. C.; van Bergen, P. F.; de Leeuw, J. W. *Geochim. Cosmochim. Acta* **1993,** *57*, 389-415.

(53) Kruge, M. A.; Bensley, D. F. In *Vitrinite Reflectance as a Maturity Parameter;* Mukhopadhyay, P. K.; Dow, W., Eds.; Amer. Chem. Soc. Symp. Series 570., 1994, pp 136-148.

(54) Gatellier, J.-P. L. A.; de Leeuw, J. W.; Sinninghe Damsté, J. S.; Derenne, S.; Largeau, C.; Metzger, P. *Geochim. Cosmochim. Acta,* **1993***, 57*, 2053-2068.

(55) George, S. C.; Jardine, D. R. *Org. Geochem.* **1994,** *21*, 829-839.

(56) Leif, R. N.; Simoneit, B. R. T. *Org. Geochem.* **1995,** *23*, 889-904.

(57) Gerard, L.; Elie, M.; Landais, P. *J. Anal. Appl. Pyrolysis* **1994**, *29*, 137-152.

(58) Vandenbroucke, M.; Behar, F.; San Torcuato, A.; Rullkötter, J. *Org. Geochem.* **1993**, *20*, 961-972.

(59) Behar, F.; Kressmann, S.; Rudkiewicz, J. L.; Vandenbroucke, M. *Org. Geochem.* **1992**,*19*, 173-189.

(60) Stankiewicz, B. A.; Kruge, M. A.; Crelling, J. C. *Bull. Centres Rech. Explor.- Prod. Elf-aquitaine* **1994**, *18*, 237-251.

(61) Hibberd, D. J. In *Handbook of Protoctista*; Margulis, L., Corliss, J. O.; Melkonian, M.; Chapman, D. J., Eds.; Jones and Bartlett: Boston, 1990; pp. 326-333.

(62) Gelin, F. (pers. comm.)

(63) Gelin, F.; de Leeuw, J. W.; Sinninghe Damsté, J. S.; Derenne, S.; Largeau, C.; Metzger, P. *Org. Geochem.* **1994**, *21*, 423-435.

(64) Flaviano, C.; Le Berre, F.; Derenne, S.; Largeau, C.; Connan, J. *Org. Geochem.* **1994**, *22*, 759-771.

(65) Pradier, B.; Landais, P.; Rochdi, A.; Davis, A. *Org. Geochem.* **1992**, *18*, 241-249.

(66) Lin R.; Ritz G. P. *Appl. Spectroscopy* **1993**, *47*, 265-271.

(67) Sinninghe Damsté, J. S.; de Leeuw, J. W. *Org. Geochem.* **1990,** *16*, 1077-1101.

(68) Tissot, B. P.; Pelet, R.; Ungerer, Ph. *AAPG Bull.* **1987**, *71*, 1445-1466.

(69) Tegelaar, E. W.; Noble, R. A. *Org. Geochem.* **1994**, *22*,543-574.

(70) Michelsen, J. K.; Khavari Khorasani, G *Org. Geochem.* **1995**, *22*, 179-189.

(71) Richnow, H. H.; Jenisch, A.; Michaelis, W. *Org. Geochem.* **1992**, *19*, 351-370.